Size Dependent Thermodynamics and Kinetics in Electric Field Mediated Colloidal Crystal Assembly

Tara D. Edwards,* Daniel J. Beltran-Villegas,* and Michael A. Bevan†
Chemical & Biomolecular Engineering, Johns Hopkins University, Baltimore, MD 21218

Supporting Information

Microscopy Experiments

Coplanar quadrupole gold thin film electrodes (Fig. S1) were patterned on glass microscope coverslips (50 mm × 24 mm × ~150 mm, Corning, Corning, NY) that were sonicated in acetone (Fisher Scientific, Pittsburgh, PA) for 30 minutes, sonicated in isopropanol (IPA, Fisher Scientific, Pittsburgh, PA) for 30 minutes, rinsed with copious amounts of deionized (DI) water, sonicated in 0.1 M potassium hydroxide (KOH, Fisher Scientific, Pittsburgh, PA) for 30 minutes, again rinsed with copious amounts of DI water, and dried with nitrogen prior to patterning. The hyperbolic quadrupole electrodes were fabricated by spin coating photoresist (S1813, Shipley Company, Marlboro, MA) onto microscope cover slips, UV exposure through a chrome photomask, and physical vapor deposition of a 10 nm chromium adhesive layer and a 40 nm gold layer. The photoresist liftoff was accomplished with agitation in 1165 Remover (Shipley Company, Marlboro, MA). The electrode tips are separated by ~100 μm. Prior to experimentation, coverslips with patterned quadrupole electrodes were sonicated in acetone for 15 minutes and IPA for 15 minutes, rinsed with copious amounts of DI H_2O, and dried with N_2.

Nominal 3.13 μm diameter SiO_2 colloids (Bangs Laboratories, Fishers, IN) were sedimentation fractionated in DI water to minimize polydispersity in experiments. Prior to each experiment, the fractionated colloidal particles in DI water were centrifuged and redispersed in 0.1 mM or 1 mM sodium hydroxide (NaOH, Sigma Aldrich, St. Louis, MO) five times to remove excess DI water and obtain dispersions of fractionated SiO_2 and NaOH.

Experiments were performed in batch cells consisting of Sylgard polydimethylsiloxane (PDMS, Dow Corning, Midland, MI) o-rings. Prior to experiments the o-rings were sonicated in IPA for 15min, rinsed with IPA, and blotted dry with lens paper (4" × 6" Fisher Scientific, Pittsburgh, PA). To construct batch cells, PDMS o-rings were coated with vacuum grease (Dow Corning, Midland, MI) and sealed between the coverslip with the patterned quadrupole electrode and a glass coverslip (18 mm × 18 mm × ~150 mm Corning, Corning, NY). 90 μL of the colloidal particle dispersion was dispensed into the batch cell and allowed to sediment for five minutes prior to sealing. 22 gauge magnet wires (Radio Shack, Fort Worth, TX) were attached to the coplanar electrode using conductive carbon tape (Ted Pella, Redding, CA). The coplanar electrode was then connected in series with a function generator (Agilent Technologies, Santa Clara, CA) with one lead attached to the north-south poles and another to the east-west poles. Table S1 summarizes experimental parameters used in PT calculations and MC simulations.

* These authors contributed equally to this work.
† Correspondence should be addressed to mabevan@jhu.edu.

Table S1. Parameters for PT calculations, MC simulations, and experiments. (a) colloidal particle size,[15, 16] (b) Debye screening length, (c) particle and wall Stern potential,[1, 2] (d) peak voltage applied to electrodes, (e) Clausius-Mosotti factor for an AC field frequency at 1 MHz,[3-5] (f) medium dielectric permittivity, (h) electrode spacing.[6-8]

Variable	Theory/Simulation	Experiment
a/nm[a]	1460	1400
κ^{-1}/nm[b]	0, 10, 30, 100	10, 30
ψ/mV[c]	-50.0	-50.0
V_{pp}/V[d]	$V(n, \kappa^{-1})$	1.0, 2.0, 3.5, 6.0, 0.7V(n, 10nm)
f_{CM}[e]	-0.2287	-0.2287
$\varepsilon_m/\varepsilon_0$[f]	78	78
d_g/μm[h]	92.95	92.95

Feedback Control over System Size

Controlling the particle number in the quadrupole has been reported by us previously.[8] In the experiments conducted in 0.1 mM NaOH, we used this ability to reduce the number of excess particles in the quadrupole upon sedimentation to a smaller specified value within ±10 particles. Briefly, the mechanism by which particles are removed from the quadrupole center employs direct current (DC) biases applied to the electrodes, resulting in simultaneous electrophoresis and electroosmosis (EPEO) to transport particles out of the quadrupole. EP transports negatively charged SiO_2 particles away from anodes towards cathodes in DC and low frequency fields, whereas EO moves particles in the opposite direction to oppose EP. As the particles travel out of the quadrupole center over to the electrode edges the particle number within the quadrupole center is reduced. Control algorithms coded in MatLab were used to remove particles from the quadrupole in batches of <25 particles at a time by making step changes to the applied AC and DC voltages based on the current number of particles.

Colloidal Potentials

We model the interaction energy between colloids in the thin film quadrupole electrode as a combination of electrostatic double layer (DLVO), induced dipole-inhomogeneous electric field (IDIF), and induced dipole-induced dipole (IDID) interactions. The gravitational potential acts in the direction normal to the underlying wall and helps confine colloids in a monolayer. As such, the net potential energy for the system is given by,

$$u_{net}(\mathbf{r}) = \sum_{i=1}^{n} u_{de,i}^{pf}(\mathbf{r}) + \sum_{<i,j>} \left(u_{e,i,j}^{pp}(\mathbf{r}) + u_{dd,i,j}^{pp}(\mathbf{r}) \right) \tag{S1}$$

where $\mathbf{r}$ is the $3n$ dimensional vector with position information for all particles in the system, $u^{pp}_{e,i,j}(\mathbf{r})$ is the electrostatic potential between particles i and j, $u^{pp}_{dd,i,j}(\mathbf{r})$ is the IDID potential between particles i and j, and $u^{pf}_{de,i}(\mathbf{r})$ is the IDIF potential of particle i. The particle-particle electrostatic potential, $u^{pp}_{e,i,j}(\mathbf{r})$, is given by,

$$u_{e,i,j}^{pp}(r_{ij}) = B^{pp} \exp\left[-\kappa \left(r_{ij} - 2a \right) \right] \tag{S2}$$

$$B^{pp} = 32\pi\varepsilon a \left(\frac{kT}{ze} \right)^2 \tanh^2 \left(\frac{ze\psi_p}{4kT} \right) \tag{S3}$$

$$\kappa = \left[\frac{\sum e^2 z_l^2 C_l N_A}{\varepsilon k T} \right]^{1/2} \tag{S4}$$

where r_{ij} is the center-to-center distance between particles, a is the particle radius, ε is the solvent dielectric permittivity, k is Boltzmann's constant, T is absolute temperature, e is the elemental charge, ψ_p is the colloid Stern potential, ψ_w is the wall Stern potential, C_l is the bulk electrolyte concentration of species l, z_l is the valence of species l, a is the particle radius, κ^{-1} is Debye length, and N_A is Avogadro's number.

IDIF and IDID interactions have been studied on the kT scale by Juarez, et al.[3-5] The IDIF interactions can be described by,

$$u_{de,i}^{pf}(\mathbf{r}) = -2kT\lambda f_\phi f_{cm}^{-1} \left(\frac{E(\mathbf{r}_i)}{E_0} \right)^2 \tag{S5}$$

where $\mathbf{r}_i$ is the position of particle i, k is Boltzmann's constant, T is the temperature, f_ϕ is a concentration dependent factor due to shielding,[9] f_{cm} is the alternating current (AC) electric field frequency dependent Clausius-Mosotti factor,[10] λ is the non-dimensional field strength, given by $\lambda=\pi\varepsilon_m a^3 (f_{cm}E_0)^2/kT$, where ε_m is the medium dielectric constant, $E(\mathbf{r}_i)$ is the electric field peak magnitude and E_0 is the nominal electric field magnitude given by $E_0=8^{-0.5}V_{pp}/d_g$, where V_{pp} is the peak-to-peak AC voltage and d_g is the gap width (between opposite electrodes). IDID interactions are given by,

$$u_{dd,i,j}^{pp}(\mathbf{r}) = -kT\lambda f_\phi P_2(\cos\theta_{ij}) \left(\frac{2a}{r_{ij}} \right)^3 \left(\frac{E(\mathbf{r}_i)}{E_0} \right)^2 \tag{S6}$$

where $P_2(\cos\theta_{ij})$ is the second Legendre polynomial and θ_{ij} is the angle between the line that connects the two particle centers and the electric field. Finally, the AC electric field in a quadrupole array is described by,[11]

$$\left| \frac{E(\mathbf{r}_i)}{E_0} \right| = \frac{4r}{d_g} \tag{S7}$$

Perturbation Theory

Perturbation theory (PT) was used to compute particle density profiles in the quadrupole electrode and determine the voltage at which all particles were crystallized. Table S1 lists the interaction potential parameters used in the PT calculations. The PT is based on an equilibrium force balance in polar coordinates,

$$\frac{1}{R}\frac{\partial}{\partial R}(R\Pi) = F(R)\rho(R) \tag{S8}$$

where R is distance from the center of the quadrupole array, Π is the colloid osmotic pressure, $\rho(R)$ is the colloid two-dimensional density profile, and $F(R)$ is the external force acting on colloids from their interaction with the AC electric field[3-5] given by,

$$F(R) = -\frac{d}{dR} u_{de,i}^{pf}(R) \tag{S9}$$

The colloid osmotic pressure, $\Pi(\rho)$, is related to the colloid number density, ρ, by,

$$\Pi(\rho) = \rho kTZ(\phi(\rho)) \tag{S10}$$

where $Z(\phi(\rho))$ is the compressibility factor, which depends on the colloid area fraction $\phi(\rho)$. $\phi(\rho)$is related to the colloid number density by, $\phi(\rho)=\rho\pi a^2$. The compressibility factor for hard disc colloidal fluids, $Z_F(\phi)$,[12] and for hard disk colloidal crystals, $Z_X(\phi)$,[13] is given by,

$$Z_F(\phi) = \left(1+\frac{\phi^2}{8}\right)(1-\phi)^{-2} \tag{S11}$$

$$Z_X(\phi) = 2\alpha^{-1} + 0.67\alpha + 1.9 \tag{S12}$$

where $\alpha=(\phi_{CP}/\phi)$-1 and ϕ_{CP}=0.907[14, 15] is the close packing area fraction for hard disks. The use of one compressibility factor over the other depends on the local area fraction. Eq (S12) is used for ϕ>0.723, and Eq. (S11) is used for ϕ<0.686.[15]

To include the effect of colloidal interactions beyond that of hard disks, we use PT to approximate repulsive potentials that effectively changes the size of particles to account for the soft repulsion past a hard wall interaction. This effective particle diameter, $2a_{eff}$, is given by,[16]

$$a_{eff} = a + \int_a^\infty \left[1 - \exp\left(-u_e^{pp}(r)/kT\right)\right] dr \tag{S13}$$

where a corresponding effective colloid area fraction, $\phi_{eff}(\rho)=\rho\pi a_{eff}^2$ can also be computed.

PT estimations of density profiles are done by numerically solving Eq (S8) and do not include the effect of IDID interactions, which have been shown to cancel out in an isotropic crystal phase.[17] This solution is obtained by assuming the particle density at a position close to the center of the gap and solving for the density at a position ∂R away using a finite difference approximation of Eq (S8). The initial density guess is iterated until the resulting density profile corresponds to the correct number of particles in the system, estimated by,

$$N = \int_0^\infty dR 2\pi R\rho(R) \tag{S14}$$

Monte Carlo Simulations

Monte Carlo (MC) simulations in the canonical ensemble are performed for n=75, 100 150, 200, 250 and 300 colloidal particles for varying applied voltages. Table S1 lists the interaction potential parameters used in all simulations. All cases explored correspond to conditions of negative values of f_{CM} so colloids are pushed towards the center of the channel rather than towards the electrodes.[3-5] These simulations were run for 10^7 steps with an initial equilibration time of $2\text{x}10^6$ steps. Configurations were stored every 10^4 steps and used to estimate ensemble averaged density profiles.

System Size Dependent Voltage Curve Fit

The results from PT calculations give the voltage at which the system will crystallize for various system sizes, n, and Debye lengths, κ^{-1}, and appear in Fig 3a and S3. To obtain a general expression, the following computations were made: (1) Linear expressions were fit to each of the $\log(V)$ as a function of $\log(n)$ data sets in Fig 3a to obtain the slope, b_0. (2) A single, two-term power law expression was fit to the voltage vs. system size in Fig S2 at each of the four Debye lengths using the b_0 values as the power. The result is a general expression for the voltage, $V(n)$, as a function of system size at the specified Debye length with the form,

$$V(n) = a_0 \cdot n^{-b_0} \tag{S15}$$

where a_0 and b_0 are constants with values at each Debye length that are given in Table S2. (3) Regression analysis was then utilized to fit a linear expression to each of the a_0 and b_0 vs. κ^{-1} data sets in Table S2. The calculated expressions for each coefficient in Eq. (S15) are,

$$\begin{aligned} a_0\left(\kappa^{-1}\right) &= 7.15 + 4.10 \cdot 10^{-3}\kappa^{-1} \\ b_0\left(\kappa^{-1}\right) &= -0.219 - 4.24 \cdot 10^{-4}\kappa^{-1} \end{aligned} \tag{S16}$$

By inserting the expressions for $a_0(\kappa^{-1})$ and $b(\kappa^{-1})$ in Eq (S16) for the individual coefficients a_0 and b_0, in Eq (S15), respectively, the expression for the voltage required for crystallization based on system size and electrostatics that appears in Eq (1) of the manuscript is obtained.

Table S2. Parameters a_0 and b_0 obtained for the voltage as a function of system size, $V(n)$ (Eq (S15)), from regression analysis fits to the data in Figs. 3 and S2 at each Debye length, κ^{-1}.

κ^{-1} (nm)	a_0 (V)	$-b_0$ (10^{-3})
0	7.22	0.22
10	7.14	0.22
30	7.22	0.23
100	7.57	0.26

Order Parameters

To characterize particle configurations, the degree of global order in particle configurations obtained from experimental particle coordinates was estimated using,[18-20]

$$\psi_{6,j} = \frac{1}{N_{C,j}} \sum_{k=1}^{N_{C,j}} e^{i6\theta_{jk}} \tag{S17}$$

$$\psi_6 = \frac{1}{j} \sum_j \psi_{6,j} \tag{S18}$$

where $\psi_{6,j}$ is the six-fold bond orientation order parameter of particle j, $N_{C,j}$ is the number of neighbors within the first $g(r)$ peak (coordination radius) of particle j, θ_{jk} is the angle between particle j and each neighboring particle with an arbitrary reference direction, and ψ_6 is the average local bond orientation order determined by averaging over all particles, which produces values between zero and one. Connectivity between crystalline particles, $\chi_{6,j}$, is given by,

$$\chi_{6,j} = \frac{\left|\mathrm{Re}\left[\psi_{6,j}\psi_{6,k}^{*}\right]\right|}{\left|\psi_{6,j}\psi_{6,k}^{*}\right|} \tag{S19}$$

where $\psi_{6,j}^{*}$ is the complex conjugate of $\psi_{6,j}$. This is used to compute the local order parameter for six-fold connectivity, $C_{6,j}$, which produces integer values between zero and six. The number of crystalline nearest neighbors, $C_{6,j}$, for particle j is determined using the criterion,[21]

$$C_{6,j} = \sum_{k=1}^{N_C(j)} \begin{bmatrix} 1 & \chi_{6,j} \geq 0.32 \\ 0 & \chi_{6,j} < 0.32 \end{bmatrix} \tag{S20}$$

$$\langle C_6 \rangle = \frac{1}{N}\sum_{i=1}^{N} C_6(i) \tag{S21}$$

where $\langle C_6 \rangle$ is the average local six-fold connectivity order, computed by averaging over all particles. This can be normalized by $\langle C_6 \rangle_{HEX}$, the six-fold connectivity order for 2D hexagonally close packed particles with a hexagonal morphology. The normalized average local six-fold connectivity order, $\langle C_6 \rangle^{*}$, produces values between zero and one and is given by,

$$\langle C_6 \rangle_{HEX} = n^{-1}6\left(3S^2 + S\right) \tag{S22}$$

$$S = -(1/2) + \left[(1/3)(n-1) + (1/4)\right]^{1/2} \tag{S23}$$

$$\langle C_6 \rangle^{*} = \langle C_6 \rangle / \langle C_6 \rangle_{HEX} \tag{S24}$$

Because of particle polydispersity uncertainty in locating particle centers due to noise, particles were considered to be nearest neighbors if they fell within an upper and lower value of the coordination radius. The coordination radius, a_{eff}=1575 nm was obtained from the first $g(r)$ peak and is equal to the core radius of the particle, a, plus several Debye lengths, x,

$$a_{eff} = a + x\kappa^{-1} \tag{S25}$$

where a is the particle radius and was found to be equal to 1400 nm from ensemble Total Internal Reflection Microscopy (TIRM)[1, 2] and x was found to be equal to 5.83 for 0.1 mM NaOH (κ^{-1}=30 nm) and 17.5 for 1 mM NaOH (κ^{-1}=10 nm). The upper bound for the coordination radius is calculated from the location of the first valley in the $g(r)$ and is equal to,

$$a_{eff}^{ub} = \left(1+\sqrt{3}\right)a_{eff} \tag{S26}$$

and the lower bound is computed using a thermal correction factor, TCF=0.92, as,

$$a_{eff}^{lb} = TCF \cdot a_{eff} \tag{S27}$$

Smoluchowski Equation Fitting Procedure

Here we outline a method to obtain $W(\mathbf{X})$ and $\mathbf{D}(\mathbf{X})$ from 2D trajectory data using Bayesian inference (BI).[22, 23] BI analysis follows a method that was reported previously[23] for a system with dynamical behavior described by two order parameters. The spatially continuous Eq. (2) in the main manuscript text can be converted into a spatially discrete master equation as,

$$\begin{aligned}\frac{dp_i(t)}{dt} = \frac{dp\left(X_l^{(1)}, X_m^{(2)}, t\right)}{dt} = -[&R\left(X_{l+1}^{(1)}, X_m^{(2)} \mid X_l^{(1)}, X_m^{(2)}\right) + R\left(X_l^{(1)}, X_{m+1}^{(2)} \mid X_l^{(1)}, X_m^{(2)}\right) + \\ &R\left(X_{l-1}^{(1)}, X_m^{(2)} \mid X_l^{(1)}, X_m^{(2)}\right) + R\left(X_l^{(1)}, X_{m-1}^{(2)} \mid X_l^{(1)}, X_m^{(2)}\right)]p\left(X_l^{(1)}, X_m^{(2)}, t\right) + \\ &R\left(X_l^{(1)}, X_m^{(2)} \mid X_{l+1}^{(1)}, X_m^{(2)}\right) p\left(X_{l+1}^{(1)}, X_m^{(2)}, t\right) + R\left(X_l^{(1)}, X_m^{(2)} \mid X_l^{(1)}, X_{m+1}^{(2)}\right) p\left(X_l^{(1)}, X_{m+1}^{(2)}, t\right) + \\ &R\left(X_l^{(1)}, X_m^{(2)} \mid X_{l-1}^{(1)}, X_m^{(2)}\right) p\left(X_{l-1}^{(1)}, X_m^{(2)}, t\right) + R\left(X_l^{(1)}, X_m^{(2)} \mid X_l^{(1)}, X_{m-1}^{(2)}\right) p\left(X_l^{(1)}, X_{m-1}^{(2)}, t\right)\end{aligned} \tag{S28}$$

where $p_i(t)$ is the probability of finding the system in a region of size $\Delta X^{(1)}\Delta X^{(2)}$ around the point i, located in $\mathbf{X}_i=(X^{(1)}_l, X^{(2)}_m)$ at time t, and the elements of the transition rate matrix, $\mathbf{R}$, express probability transition rates between adjacent regions. Eq. (S28) can be solved in terms of a matrix exponential of the rate matrix as,

$$p_i(t) = p\left(X_l^{(1)}, X_m^{(2)}, t\right) = \sum\nolimits_j e_{ij}^{t\mathbf{R}}\, p_j(0) \tag{S29}$$

where $p_j(0)$ is the initial condition for Eq. (S28). The matrix exponential $e^{t\mathbf{R}}$ defines transition probabilities between regions i, located in $\mathbf{X} = \mathbf{X}_i$, and j, located in $\mathbf{X} = \mathbf{X}_j$, as,

$$p\left(\mathbf{X}_i, t \mid \mathbf{X}_j, 0\right) = e_{ij}^{t\mathbf{R}} \tag{S30}$$

Given that the master equation, Eq. (S28), obeys detail balance, the number of parameters can be reduced. This condition states that $R_{ij}p^{\mathrm{eq}}(\mathbf{X}_j) = R_{ji}p^{\mathrm{eq}}(\mathbf{X}_i)$, where,

$$p^{eq}\left(\mathbf{X}_i\right) = p_0 \exp\left[-\frac{W(\mathbf{X}_i)}{kT}\right] \tag{S31}$$

where p_0 is a constant prefactor. Additionally, the elements of the rate matrix $\mathbf{R} = [R_{ij}]$ satisfy $R_{ij} \geq 0$ for $i \neq j$, $R_{ij} < 0$ for $i = j$, and $\Sigma_j R_{ij} = 0$. Finding the solution of Eq. (S30) is accomplished by following the procedure described by Hummer.[22] The relation between the rate matrix $\mathbf{R}$ and Smoluchowski equation coefficients, is given by,[23]

$$R_{k+1,l|k,l} = -\left(\frac{D^{(1)(1)}\alpha_1}{\Delta X^{(1)}} + \frac{D^{(1)(2)}\alpha_2}{\Delta X^{(2)}}\right)\frac{1}{\left(e^{-\alpha_1} - 1\right)\Delta X^{(1)}} \tag{S32}$$

$$R_{k,l|k+1,l} = \left(\frac{D^{(1)(1)}\alpha_1}{\Delta X^{(1)}} + \frac{D^{(1)(2)}\alpha_2}{\Delta X^{(2)}}\right)\frac{1}{\left(e^{\alpha_1} - 1\right)\Delta X^{(1)}} \tag{S33}$$

$$R_{k,l+1|k,l} = -\left(\frac{D^{(2)(1)}\alpha_1}{\Delta X^{(1)}} + \frac{D^{(2)(2)}\alpha_2}{\Delta X^{(2)}}\right)\frac{1}{\left(e^{-\alpha_2} - 1\right)\Delta X^{(2)}} \tag{S34}$$

$$R_{k+1,l|k,l} = \left(\frac{D^{(2)(1)}\alpha_1}{\Delta X^{(1)}} + \frac{D^{(2)(2)}\alpha_2}{\Delta X^{(2)}}\right)\frac{1}{\left(e^{\alpha_2} - 1\right)\Delta X^{(2)}} \tag{S35}$$

$$\alpha_1 = \frac{f_1\Delta X^{(1)}}{kT} \text{ and } \alpha_2 = \frac{f_2\Delta X^{(2)}}{kT} \tag{S36}$$

and f_1 and f_2 are local "forces" given by,

$$f_1 = -\frac{W\left(X_{l+1}^{(1)}, X_m^{(2)}\right) - W\left(X_l^{(1)}, X_m^{(2)}\right)}{\Delta X^{(1)}} \text{ and } f_2 = -\frac{W\left(X_l^{(1)}, X_{m+1}^{(2)}\right) - W\left(X_l^{(1)}, X_m^{(2)}\right)}{\Delta X^{(2)}} \quad \text{(S37)}$$

and $D^{(u)(v)}$ is the *uv*-component of the diffusivity tensor. The Smoluchowski equation coefficients, $W(\mathbf{X})$ and $\mathbf{D}(\mathbf{X})$, can be estimated from a set of dynamic observations by estimating the variability of the likelihood function,

$$L \equiv \prod_{\beta} p\left(\mathbf{X}_{i_\beta}, t_{k_\beta} \mid \mathbf{X}_{j_\beta}, 0\right) \quad \text{(S38)}$$

where β refers to a realization of the system. This variability is sampled based on the Metropolis Monte Carlo algorithm varying the values of $W(\mathbf{X})$ and $\mathbf{D}(\mathbf{X})$. From $W(\mathbf{X})$ and $\mathbf{D}(\mathbf{X})$, the master equation parameters p^{eq} and $\mathbf{R}$ are calculated using Eqs. (S31), (S32)-(S35). These parameters are used to numerically solve the equivalent master equation to get transition probabilities, $p(\mathbf{X}_i,t_k|\mathbf{X}_j,0)$. The negative log-likelihood ($-\ln L$) is used as the energy function in the Monte Carlo procedure as,

$$-\ln L = -\sum_k \sum_j \sum_i N\left(\mathbf{X}_i, t_k \mid \mathbf{X}_j, 0\right) \ln p\left(\mathbf{X}_i, t_k \mid \mathbf{X}_j, 0\right) \quad \text{(S39)}$$

where $N(\mathbf{X}_i,t_k|\mathbf{X}_j,0)$ is a jump matrix that has information of observed number of jump between state $\mathbf{X}_j$ and state $\mathbf{X}_i$ after t_k time. The algorithm output provides a range of converged values for both functions $W(\mathbf{X})$ and $\mathbf{D}(\mathbf{X})$ from which the average and standard deviation can be estimated.

As far as implementation details, jump matrices, $N(\mathbf{X}_i,t|\mathbf{X}_j,0)$, were constructed by counting the number of transitions from all initial positions to all final positions in **X**-phase space for different jump times, t. Jump times ranged from t = 6,250 s to t = 31,250 s. **X** space was discretized to have a total number of regions equal or less than 100. An initial guess for $W(\mathbf{X})$ was based on the Boltzmann inverted FEL, $W_{guess}(\mathbf{X})=-\ln[h(\mathbf{X})]$, where $h(\mathbf{X})$ denotes the sampling histogram of states from experiment data. The initial guess for $\mathbf{D}(\mathbf{X})$ was set to a constant of 10^{-10} for all values and components. Metropolis Monte Carlo runs, varying $W(\mathbf{X})$ and $\mathbf{D}(\mathbf{X})$, used a given jump matrix, $N(\mathbf{X}_i,t|\mathbf{X}_j,0)$, and were run for 10^8 steps with an output writing frequency of 10^4 steps. Reported values of $W(\mathbf{X})$ and $\mathbf{D}(\mathbf{X})$ were calculated as the mean value of the resulting run after the energy function (Eq (S39)) reached a plateau. The resulting run also had information on the uncertainty of the Smoluchowski equation parameters, which were estimated as the variance of the values used to determine the reported mean.

References

1. Wu, H. J.; Bevan, M. A., Direct Measurement of Single and Ensemble Average Particle-Surface Potential Energy Profiles. *Langmuir* **2005,** 21, (4), 1244-1254.
2. Wu, H.-J.; Pangburn, T. O.; Beckham, R. E.; Bevan, M. A., Measurement and Interpretation of Particle−Particle and Particle−Wall Interactions in Levitated Colloidal Ensembles. *Langmuir* **2005,** 21, (22), 9879-9888.
3. Juarez, J. J.; Bevan, M. A., Electric Field Induced Colloidal Interactions and Equilibrium Microstructures. *J. Chem. Phys.* **2009,** 131, 134704.
4. Juarez, J. J.; Cui, J.-Q.; Liu, B. G.; Bevan, M. A., kT-Scale Colloidal Interactions in High Frequency Inhomogeneous AC Electric Fields. I. Single Particles. *Langmuir* **2011,** 27, (15),

9211-9218.
5. Juarez, J. J.; Liu, B. G.; Cui, J.-Q.; Bevan, M. A., kT-Scale Colloidal Interactions in High-Frequency Inhomogeneous AC Electric Fields. II. Concentrated Ensembles. *Langmuir* **2011,** 27, (15), 9219-9226.
6. Juarez, J. J.; Feicht, S. E.; Bevan, M. A., Electric field mediated assembly of three dimensional equilibrium colloidal crystals. *Soft Matter* **2012,** 8, (1), 94-103.
7. Juarez, J. J.; Bevan, M. A., Feedback Controlled Colloidal Self-Assembly. *Advanced Functional Materials* **2012,** 22, (18), 3833-3839.
8. Juarez, J. J.; Mathai, P. P.; Liddle, J. A.; Bevan, M. A., Multiple electrokinetic actuators for feedback control of colloidal crystal size. *Lab on a Chip* **2012,** 12, (20), 4063-4070.
9. Adriani, P. M.; Gast, A. P., A microscopic model of electrorheology. *Phys. Fluids* **1988,** 31, (10), 2757-2768.
10. Saville, D. A.; Bellini, T.; Degiorgio, V.; Mantegazza, F., An extended Maxwell--Wagner theory for the electric birefringence of charged colloids. *J. Chem. Phys.* **2000,** 113, (16), 6974-6983.
11. Pethig, Y. H. a. R., Electrode design for negative dielectrophoresis. *Measurement Science and Technology* **1991,** 2, (12), 1142.
12. Henderson, D., Monte carlo and perturbation theory studies of the equation of state of the two-dimensional Lennard-Jones fluid. *Molecular Physics* **1977,** 34, (2), 301-315.
13. McBride, C.; Vega, C., Fluid solid equilibrium for two dimensional tangent hard disk chains from Wertheim's perturbation theory. *Journal of Chemical Physics* **2002,** 116, (5), 1757-1759.
14. Mitus, A. C.; Weber, H.; Marx, D., Local structure analysis of the hard-disk fluid near melting *Phys. Rev. E* **1997,** 55, (6), 6855-6859.
15. Huerta, A.; Henderson, D.; Trokhymchuk, A., Freezing of two-dimensional hard disks. *Physical Review E* **2006,** 74, (6).
16. Beckham, R. E.; Bevan, M. A., Interfacial Colloidal Sedimentation Equilibrium I. Intensity based Confocal Microscopy. *J. Chem. Phys.* **2007,** 127, 164708.
17. Khusid, B.; Acrivos, A., Effects of interparticle electric interactions on dielectrophoresis in colloidal suspensions. *Phys. Rev. E* **1996,** 54, (5), 5428.
18. Fernandes, G. E.; Beltran-Villegas, D. J.; Bevan, M. A., Interfacial Colloidal Crystallization via Tunable Hydrogel Depletants. *Langmuir* **2008,** 24, 10776-10785.
19. Fernandes, G. E.; Beltran-Villegas, D. J.; Bevan, M. A., Spatially Controlled Reversible Colloidal Self-Assembly. *J. Chem. Phys.* **2009,** 131, 134705.
20. Nelson, D. R.; Halperin, B. I., Dislocation-mediated melting in two dimensions. *Phys. Rev. B* **1979**, 2457-2484.
21. ten Wolde, P. R.; Ruiz-Montero, M. J.; Frenkel, D., Numerical calculation of the rate of crystal nucleation in a Lennard-Jones system at moderate undercooling. *J. Chem. Phys.* **1996,** 104, 9932.
22. Hummer, G., Position-dependent diffusion coefficients and free energies from Bayesian analysis of equilibrium and replica molecular dynamics simulations. *New J. Phys.* **2005,** 7, 34.
23. Beltran-Villegas, D. J.; Sehgal, R. M.; Maroudas, D.; Ford, D. M.; Bevan, M. A., Colloidal cluster crystallization dynamics. *The Journal of Chemical Physics* **2012,** 137, (13), 134901.

Figure S1

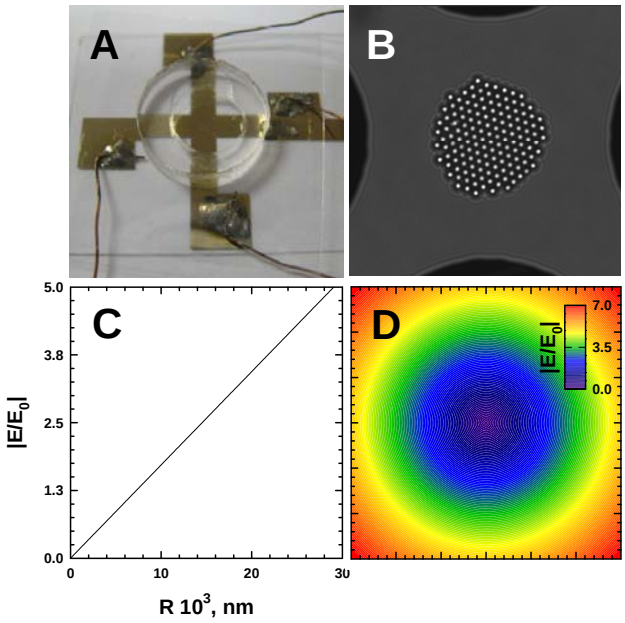

Experimental configurations for silica colloids in high frequency AC electric fields and radial dependence of electric field expression used in simulation calculations. (A) Au film quadrupole electrodes on a glass microscope slide with PDMS o-ring containing an aqueous colloidal dispersion. Electrodes are connected in series to a function generator operated by computer software. (B) Optical microscopy/charged coupled device image of quasi-2D crystal of 3 μm silica colloids in quadrupole center. (C) Non-dimensional electric field magnitude in the quadrupole as a function of distance from the center of the gap, *R*. (D) Contour plot of electric field used in simulations with linear spectrum scale from $E/E_0 = 0$ to $E/E_0 = 7$.

Figure S2

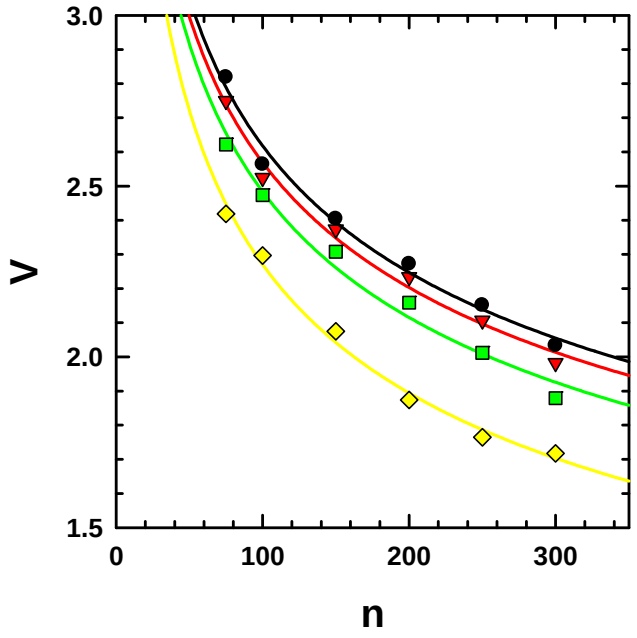

Voltage, V, required for quasi-2D crystallization from PT calculations at system sizes, n, equal to 75, 100, 150, 200, 250, and 300 particles. Calculations conducted at each system size for ionic strength conditions of κ^{-1}=0 nm (black circles), 10 nm (red inverted triangles), 30 nm (green squares), 100 nm (yellow diamonds). Solid lines correspond to $V(n)$ obtained from fitting a single, two-term power law expression to the points from PT results at each of the four Debye lengths using regression analysis. Lines and points have the same color at a given Debye length.